

# Sequential Synthesis of Type II Colloidal CdTe/CdSe Core–Shell Nanocrystals

Kui Yu,\* Badruz Zaman, Svetlana Romanova, Da-shan Wang, and John A. Ripmeester

**C**olloidal type II CdTe/CdSe nanocrystals were synthesized by sequential addition of a tri-*n*-octylphosphine telluride (TOPTe)/TOP solution and several shell-precursor solutions to a CdO/TOP solution; the shell-precursor solutions consisted of CdO and TOPSe in TOP. For the growth of the CdTe core, the TOPTe/TOP solution was swiftly added to the CdO/TOP solution at a higher temperature (300°C) than the growth temperature (250°C). For the growth of the CdSe shell, in contrast, the CdO/TOPSe/TOP solution was slowly added to the CdTe/TOP solution at a lower temperature than the growth temperature (200–240°C). The temporal evolution of the optical properties of the growing core–shell nanocrystals was monitored in detail. During the growth of the CdSe shell, the core–shell nanocrystals exhibited interesting changes in photoluminescence (PL) properties. The highest PL efficiency ( $\approx 38\%$ ) was detected from core–shell nanocrystals with a CdSe shell thickness of 0.4–0.5 nm (indicated by TEM); the formation of the first monolayer is proposed. Our synthetic approach is well suited to a practical realization of engineering materials with bandgaps in the near-IR and IR spectral ranges.

## Keywords:

- core–shell materials
- nanocrystals
- photoluminescence
- semiconductors
- synthesis

## 1. Introduction

Recently, the synthesis of heterostructured semiconductor nanocrystals has become an active field; not only is this line of research important today, but it is likely to attract a great deal of attention in the immediate future with applica-

tions including photovoltaics and optoelectronic devices.<sup>[1]</sup> Wet-chemical preparations have demonstrated their suitability for the fabrication of heterostructured nanocrystals, such as type I and type II nanocrystals, where a higher bandgap shell material is grown onto a core material with a lower bandgap.<sup>[2–6]</sup> For type I nanocrystals, the band offsets are such that the conduction and valence bands of the shell are of higher and lower energy than those of the core, respectively, while for type II nanocrystals they are such that the energies of the conduction and valence bands of the shell are either both higher or both lower than those of the core. Consequently, the type II materials (AX/BY) can spatially separate and confine photogenerated holes and electrons. The recombination of the electron–hole pair due to Coulombic attraction between electrons and holes (tunneling through the AX/BY interface) can be radiative; the energy of their emission depends on the band offset ( $\Delta E_v$ ), which is smaller than the bandgap of both AX and BY. Therefore,

[\*] K. Yu, B. Zaman, S. Romanova, J. A. Ripmeester  
Steacie Institute for Molecular Sciences  
National Research Council of Canada  
Ottawa, Ontario K1A 0R6 (Canada)  
Fax: (+1) 613-998-7833  
E-mail: kui.yu@nrc.ca

D.-s. Wang  
Institute for Chemical Process and Environmental Technology  
National Research Council of Canada  
Ottawa, Ontario K1A 0R6 (Canada)

Supporting information for this article is available on the WWW under <http://www.small-journal.com> or from the author.

the type II materials are engineered by the band offset as well as the dimensions of each single component.

A common-cation system, CdTe (core)/CdSe (shell) nanocrystals are type II materials with spatially indirect interband transitions, where the majority of photogenerated holes are confined in the CdTe core and the electrons in the CdSe shell, as demonstrated in Figure 1.<sup>[5,6]</sup> The natural va-

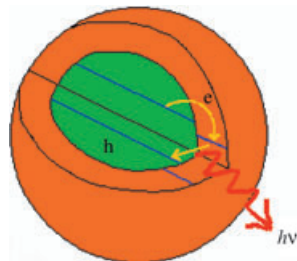


**Figure 1.** Schematic drawing of a CdTe/CdSe core(shell) nanocrystal. Upon radiation, the charge carriers can be spatially separated: the hole (h) is mostly confined in the CdTe core and the electron (e) in the CdSe shell. The recombination of the hole and the electron can be radiative.

lence-band offset ( $\Delta E_v$ ) was calculated as 0.57 eV.<sup>[5]</sup> The photoemission red shift of the core-shell nanocrystal (shown in Figure 1, as compared to the photoemission of the core nanocrystal) is related strongly to the CdSe shell thickness. Furthermore, the photoluminescence (PL) efficiency of the CdTe/CdSe nanocrystal is strongly related to the PL efficiency of the CdTe core and the shell thickness; a thinner shell was argued to give a higher PL efficiency, due to a better overlap of the hole and electron wave functions.<sup>[6]</sup>

A synthetic route to CdTe/CdSe colloidal nanocrystals was first reported in 2003.<sup>[6]</sup> The CdTe core was synthesized via the traditional pyrolysis of organometallic precursors and was precipitated and dispersed in tri-*n*-octylphosphine oxide (TOPO); afterwards, dimethylcadmium ( $\text{CdMe}_2$ ) and bis-(trimethylsilyl)selenide (1:1 molar ratio in tri-*n*-octylphosphine (TOP)) was added into the CdTe/TOPO dispersion for the growth of the CdSe shell at 130–180 °C. The PL efficiency (quantum yield (QY)) was claimed to be less than 4% for those CdTe/CdSe nanocrystals prepared.

In the present study, we report on a much simpler synthesis of CdTe/CdSe nanocrystals but resulting in a much higher QY. With CdO as the Cd source, the synthesis of colloidal II–VI nanocrystals in TOP has recently been extensively investigated in our laboratories.<sup>[7]</sup> The synthetic approach to CdTe/CdSe core-shell nanocrystals involves the sequential addition of a TOPTe/TOP solution and several CdO/TOPSe/TOP solutions (so-called shell-precursor solutions) to a CdO/TOP solution. No acids, amines, or TOPO were added, neither was precipitation of core CdTe nanocrystals involved. Furthermore, we report on the growth kinetics of the CdSe shell via monitoring the temporal evolution of the optical properties during the growth of the CdSe shell. Such careful examination of the temporal evolution of the optical properties of the resulting core-shell nanocrystals

is expected to be very rewarding for targeting high-quality CdTe/CdSe core-shell nanocrystals with high PL efficiency. In addition, it will lead to a better fundamental understanding of the effects of surface passivation in the early stage of the “island growth” affecting the quantum efficiency,<sup>[8]</sup> and the effects of the later-stage shell growth affecting the charge-carrier separation and the quantum efficiency. The hope is that such an investigation may bring insight for rational design strategies toward bandgap engineering, that is, to tune the heterostructured nanocrystal bandgap to be in the near-IR and IR spectral ranges for various promising applications.<sup>[3–6]</sup>

## 2. Results

Our synthetic approach successfully prevents the formation of CdSe nanocrystals and produces high-quality CdTe/CdSe nanocrystals. The approach is similar to sequential anionic polymerization for well-defined diblock copolymers,<sup>[9–11]</sup> such as polystyrene-*block*-poly(ethylene oxide) (PS-*b*-PEO), particularly regarding the addition of the TOPTe/TOP solution and subsequently the shell-precursor solutions (compare with the addition of the first block monomer (styrene) and the subsequent addition of the second block monomer (EO)).<sup>[10,11]</sup> During the sequential anionic polymerization of PS-*b*-PEO, the PS block is polymerized first via the addition of styrene monomer into a reaction medium consisting of tetrahydrofuran (THF) with cumyl potassium as the initiator. Without precipitation for purification of the PS block, EO monomer is added for the engineering of the PS-*b*-PEO diblock copolymer with low polydispersity. In order to minimize the formation of poly(ethylene oxide) homopolymer, the addition of the EO monomer needs to be carried out dropwise under efficient stirring. Before the addition of EO, an aliquot of the reaction medium is usually withdrawn for the characterization of the PS block length and polydispersity by size-exclusion chromatography (SEC). Also, the growth of the diblock block is monitored until the desired EO block length is achieved.<sup>[11]</sup>

Similar ideas on the sequential addition of styrene and EO monomers as well as the on-line monitoring of the block length of the homo-PS block and the diblock PS-*b*-PEO are extended to synthesize our CdTe/CdSe nanocrystals; efforts were also made to prevent the nucleation and growth of the CdSe nanocrystals. In general, for the synthesis of CdTe/CdSe core-shell nanoparticles, a TOPTe/TOP solution (stock solution 1) was injected into in a reaction flask consisting of a CdO/TOP solution for the growth of CdTe. Afterwards, a TOPSe/CdO/TOP solution (stock solution 2; shell-precursor solution) was injected into the reaction flask containing the CdTe/TOP solution for the growth of CdSe shell. Table 1 summarizes the stock solutions that were prepared. Similar to the on-line monitoring of the copolymer block length and polydispersity, we monitored the temporal evolution of the optical properties of the growing nanocrystals.

The as-prepared CdTe core exhibited photoemission at  $\approx 666$  nm, with a full width at half-maximum (FWHM) of

**Table 1.** Stock solutions prepared for the sequential synthesis of type II CdTe/CdSe nanocrystals.

Chemicals	Stock solution			
	1	2	3	4
Te(mg)/TOP(g)	12.76/0.798			
CdO(mg)/TOP(g)		12.86/1.496	16.59/1.945	16.59/1.945
Se(mg)/TOP(g)		7.88/0.170	10.24/0.222	10.24/0.222
Cd or Se (mmol)		0.1	0.13	0.13
Cd or Se (mmol kg <sup>-1</sup> )		59	59	59

≈47 nm and a PL QY of ≈31% (see Supporting Information for QY characterization). CdTe nanocrystals with a high QY are essential for the preparation of CdTe/CdSe core-shell materials: the precipitation of colloidal II-VI nanocrystals usually results in a significant decrease in PL QY, due to surface ligand removal;<sup>[12a]</sup> in addition, Te is very sensitive to oxygen.<sup>[12b,c]</sup> Consequently, sequential addition of the shell-precursor materials directly to the synthetic-core solution is believed to be crucial.

The temporal evolution of the optical properties during the growth of the CdSe shell (after the injection of stock solution 2) was monitored in detail and is presented in Figure 2, with the emission (left, 3-dimensional) and absorp-

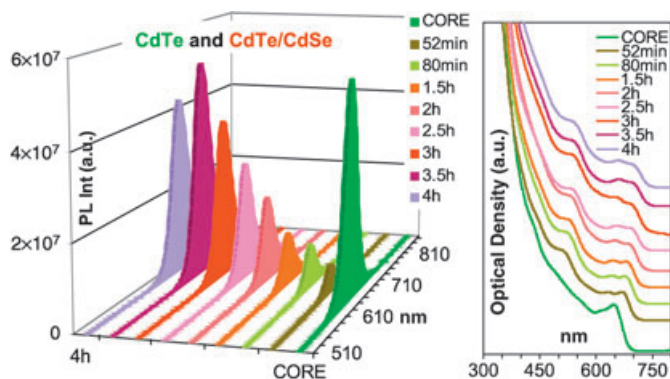


**Figure 2.** Temporal evolution of the PL spectra (left, m-corrected) and the UV/vis absorption spectra (right) of the CdTe core nanocrystals and the CdTe/CdSe nanocrystals. The different growth periods of the core-shell nanocrystals sampled from the reaction flask after the injection of stock solution 2, namely a CdO/TOPSe/TOP solution with a 1:1 Cd/Se molar ratio, are indicated. The nanocrystals were dispersed in hexane.

tion spectra (right) of both the as-prepared CdTe and the as-prepared CdTe/CdSe nanocrystals. The presence of CdSe nanocrystals could not be detected from the emission spectra after the injection of stock solution 2 and during the growth of the CdSe shell. An enhancement of the emission intensity was observed throughout a growth period of the CdSe island (or layer) up to 3.5 h, which was accompanied by considerable red shifts of the emission maxima; at the same time, the feature of the absorption peak close to the first exciton peak became more sharp.

Figure 3A summarizes the growth kinetics of the CdSe shell, namely, red shifts of the absorption (○) and emission

(●) peak positions of the growing nanocrystals (after the injection of stock solution 2). After the injection of stock solution 2, the reaction solution was heated from 140 to 200°C: the rate of the temperature increase is an important factor for preventing the growth of CdSe nanocrystals. After 27 min, CdTe/CdSe nanocrystals (sampled at 162°C) exhibited a PL maximum at ≈665 nm and FWHM of ≈41 nm,

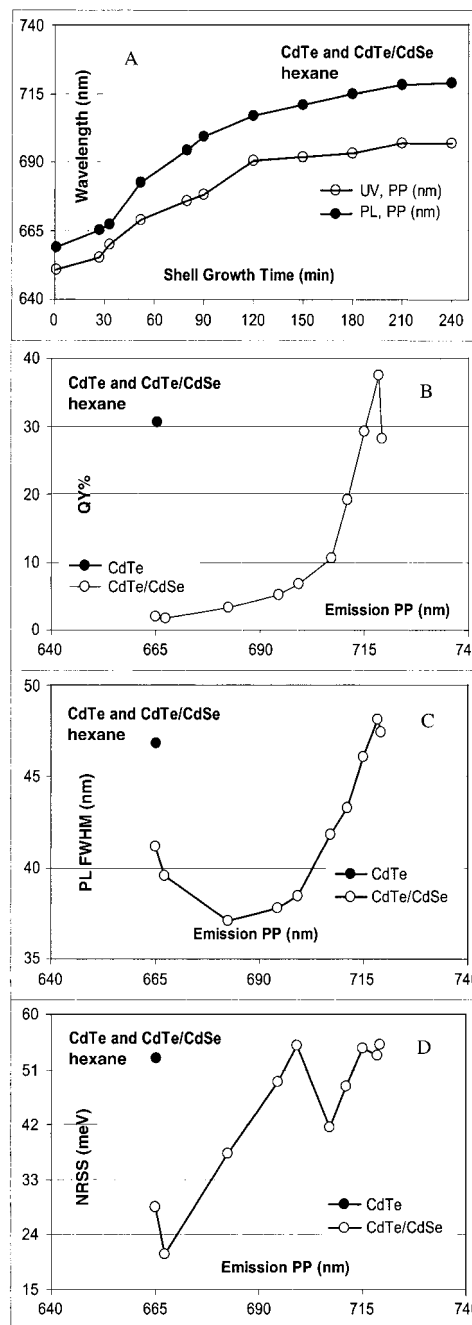


**Figure 3.** Temporal evolution of: A) the bandgap peak positions (PP, wavelength in nm) of the absorption (○) and emission (●); B) the quantum yield based on Dye R590; C) the FWHM values; D) the NRSS of the CdTe (● in B–D)) and growing CdTe/CdSe nanocrystals (○ in the B–D)) from the reaction whose results were shown in Figure 2.

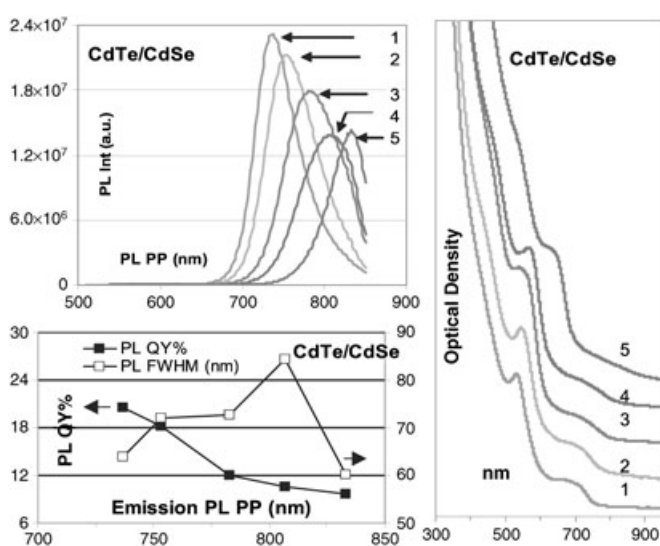
while after 33 min, the nanocrystals (at 177 °C) displayed a PL maximum at  $\approx 667$  nm and FWHM of  $\approx 40$  nm. After 52 min, the temperature had reached 192 °C and from this point, the red shift became more pronounced up to reaction periods of 2.5 h (at 200 °C). During growth from 52 to 150 min, the PL maximum shifted from  $\approx 682$  nm to  $\approx 715$  nm.

Figure 3B summarizes the change of the PL efficiency from the CdTe nanocrystals (●) to the growing CdTe/CdSe nanocrystals (○), estimated as the quantum yield based on dye R590. In general, a substantial decrease of the PL efficiency was immediately detected after the addition of stock solution 2; this was followed by a significant enhancement of the PL efficiency during  $\approx 3$  h growth of a CdSe layer.

Interestingly, the patterns of the temporal evolution of the PL efficiency and that of the PL FWHM (Figure 3C) are similar; hence, we believe that the temporal change of the PL FWHM is related to the nanoparticle surface; Ostwald ripening of the CdTe core during the shell growth was limited, as evidenced by transmission electron microscopy (TEM). The PL technique has been used to characterize the interface roughness of quantum well structures, such as ZnSe/CdSe fabricated by molecular beam epitaxy (MBE);<sup>[8]</sup> the linewidth of excitonic emission is related to the lateral dimensions of islands and valleys at the well interface.<sup>[13]</sup> Furthermore, we have observed that identical CdSe or CdTe nanoparticles can exhibit different PL FWHM values, depending on their dispersing media, such as hexane or THF; such a difference should be related to different degrees of surface ligand removal in hexane and THF.<sup>[7]</sup> The energy difference between the bandgap peaks of the absorption and emission is the so-called non-resonant Stokes shift (NRSS),<sup>[14]</sup> whose values are influenced by nanocrystal size, shape, and distribution. The present nanocrystals exhibit a NRSS between 20 to 55 meV, as shown in Figure 3D; the pattern of the temporal change of the NRSS has some similarity to those of the PL efficiency and PL FWHM. We believe that the NRSS is one of the parameters also affected by the surface quality of nanocrystals.<sup>[7]</sup>

During the 3.5–4 h reaction period, a red shift of less than 1 nm (718.5 nm to 719.3 nm) was detected along with a considerable decrease in the PL efficiency. In order to further tune the photoemission to longer wavelength, we prepared stock solution 3, which consisted of CdO (0.13 mmol), TOPSe (0.13 mmol), and TOP (2.2 g), with a Se concentration of  $\approx 59$  mmol kg<sup>-1</sup>. After the reaction flask was cooled to 180 °C, stock solution 3 was injected dropwise into the reaction flask. After 30 min, the reaction flask was heated back to 200 °C. As shown in Figure 4 (curve 1), CdTe/CdSe nanocrystals grown for 60 min (after the addition of stock solution 3) exhibited a PL maximum at  $\approx 737$  nm. Since a red shift of only  $\approx 1$  nm was detected for the next 30 min at 200 °C, the reaction solution was heated to 225 °C; the nanocrystals then exhibited a PL maximum at  $\approx 753$  nm (Figure 4; curve 2).

We then prepared stock solution 4, which had the same constituents as stock solution 3. After the dropwise addition of this solution, the emission spectra of the samples grown for 3.5 h (after the addition of stock solution 4 and sampled



**Figure 4.** PL spectra (left top, m-corrected to 850 nm, which corresponds to the instrument limit. See Supporting Information for the corresponding non-corrected spectra) of the CdTe/CdSe nanocrystals sampled after the injection of stock solutions 3 and 4, and the corresponding UV/vis absorption spectra (right) in hexane. The QY and the PL FWHM are indicated in the lower left section.

at 200 °C), 7 h (225 °C), and 13 h (238 °C) were recorded (Figure 4; curves 3–5).<sup>[15]</sup> The corresponding non-corrected PL spectra are available in the Supporting Information, and the description of the m-correction is given in the Experimental Section.

The prepared nanocrystals were directly imaged by transmission electron microscope (TEM). It is known that TEM is a powerful characterization tool for obtaining information on morphology and size distributions; high-resolution TEM can distinguish between crystalline and amorphous materials, and can provide lattice information such as crystal type, structure, orientation, and defects. Representative bright-field TEM images (Figure 5) and HRTEM images (Figure 6) of the CdTe cores and of CdTe/CdSe nanocrystals grown for 3.5 h (whose PL was displayed in Figure 2) and for 13 h (whose PL was displayed in Figure 4; curve 5) are shown as parts of A, B, and C in Figures 5 and

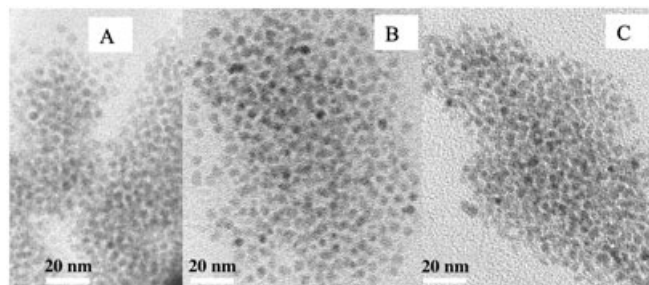


**Figure 5.** TEM images of the CdTe cores (A), CdTe/CdSe nanocrystals obtained after 3.5 h (B), whose PL spectra are shown in Figure 2, as well as the core-shell nanocrystals (C), whose PL spectrum is shown in Figure 4 (curve 5).

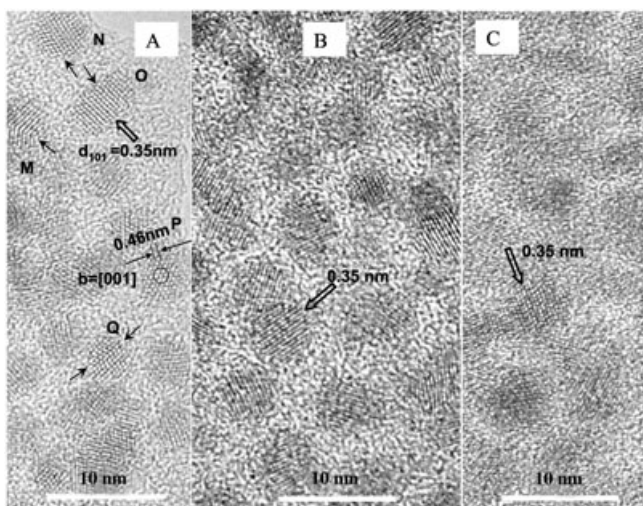


Figure 6. HRTEM images of the CdTe cores (A), CdTe/CdSe nanocrystals obtained after 3.5 h (B), and the core-shell nanocrystals obtained after 13 h (C).

6, respectively. As measured from the TEM images, the sizes of the nanocrystals shown in Parts A, B, and C in Figure 5 are 3.2–4.5 nm, 4.0–5.5 nm, and 4.3–7.5 nm in diameter, respectively. Such an increase in size clearly demonstrates the success of the CdSe coating, since CdTe nanocrystals with diameters less than 7.5 nm exhibit photoemission below 750 nm.<sup>[12c]</sup>

The crystalline structure of individual particles can be determined by carefully examining the two-dimensional lattice structure and by measuring the lattice spacings (in HRTEM images). For example, a hexagon can be drawn by arbitrarily choosing one spot and the other six closest neighboring spots, as shown for particle P in Figure 6a; the spacing between two neighboring spots was measured to be  $\approx 0.46$  nm, which agrees with the lattice parameter  $a_0 = 0.457$  nm of the wurtzite form of CdTe.<sup>[16]</sup> Therefore the zone axis of the particle can be determined to be [001]. Another typical  $d$  spacing was measured to be 0.35 nm in particle O, which again matches the wurtzite structural of CdTe ( $d_{(101)} = 0.352$  nm). Note that a two-dimensional lattice image can not always be exhibited due to the random orientation of the particles on the TEM grid. Only those in which a specific zone axis is exactly parallel to the electron beam may possibly display two-dimensional lattice periodicity, arrayed with spots representing columns of atoms in the crystal projected onto the image plane; otherwise, nanocrystals will exhibit either equally spaced fringes representing the projection of crystal planes or no lattice information.

Defects such as stacking faults and twins were also identified. Examples of twin boundaries in the CdTe nanoparticles of Figure 6a are indicated with arrows in particles M, N, and Q, and an example of an ABBA stacking fault is observed in particle O. The formation mechanism of the crystal defects is uncertain. From the point of view of nucleation, the default areas are possibly the pioneer nuclei for further growth of the particles. A similar analysis can be

conducted on the core-shell particles shown in Figure 6B and C for crystallographic information.

The size increase for the particles shown in Figure 5, as mentioned above, is due to the coating of the CdSe shell onto the CdTe core. However, it is difficult to determine the boundary between the CdTe core and the CdSe shell. Because of the fact that TOP/CdSe and TOP/CdTe nanocrystals prepared via our synthetic approach (from a reaction media consisting of TOP without other additives) have the same wurtzite structure with a small difference in their lattice parameters (Figure 7), it is difficult to recognize the in-

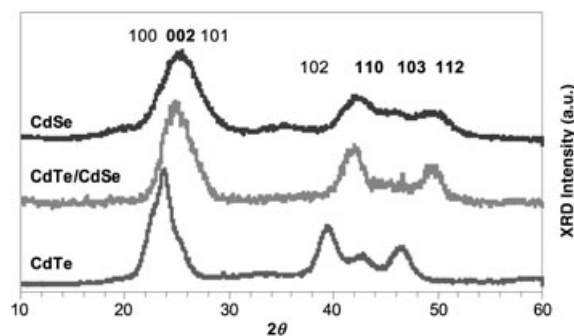


Figure 7. X-ray diffraction patterns from CdSe, CdTe/CdSe, and CdTe nanocrystals synthesized from our TOP reaction media. The core-shell nanocrystal exhibited PL at 839 nm.

terface by image contrast, even if a sharp interface exists between the core and shell due to an interruption in composition (from epitaxial growth). Furthermore, the CdTe core and CdTe/CdSe nanocrystals shown in Figure 5A and B are much more spherical in shape than those shown in Figure 5C. In addition, more twinlike crystal grains are observed from Figure 5C. It is possible that some of the twin grains represent the CdTe/CdSe interface (but not from epitaxial growth).

### 3. Discussion

For materials on the nanometer scale, it is easier to show that they work than to explain how they work. It is obvious that this sequential synthetic approach to CdTe/CdSe nanocrystals is facile, without any precipitation or purification of the CdTe core, and that it produces high-QY core-shell nanoparticles. In addition, it would be of help to correlate the CdSe shell thickness with the red shift and QY of the core-shell nanocrystals, in order to provide useful knowledge for the bandgap engineering of type II core-shell nanocrystals.

Let us review briefly the properties of the CdTe and CdTe/CdSe nanocrystals reported in 2003:<sup>[6]</sup> CdTe nanocrystals, with a diameter of  $\approx 6.4$  nm, exhibited PL at  $\approx 670$  nm with a FWHM of  $\approx 30$  nm; with a 1.1 nm coating of CdSe, the resulting CdTe/CdSe nanocrystals exhibited a PL maximum at  $\approx 843$  nm with a FWHM of  $\approx 95$  nm. If the shell thickness of one CdSe layer is expected to be  $\approx 0.7$  nm,<sup>[17]</sup>

the reported CdTe/CdSe nanocrystals that exhibit PL at 843 nm seem to have a shell comprised of  $\approx 1.6$  monolayers.

Regarding TOP-capped CdTe/CdSe nanocrystals, a comprehensive understanding of the temporal evolution of their optical behavior remains elusive; however, based on their optical properties, it seems that after the addition of stock solution 2 and by heating the reaction solution from 140 to 177 °C, there was little growth of the CdSe shell. The addition of stock solution 2 caused a dilution effect: surface ligands such as TOPTe partially dissociated, which resulted in a slight blue shift of the PL maximum and a considerable decrease of the PL efficiency. When the temperature reached 192 °C after 52 min, the growth of the CdSe coating became more pronounced, with a significant enhancement of the PL efficiency as well as obvious red shifts in the PL maximum. During this period of coating, the formation of the CdSe shell as (monolayer) islands and structural disorder at the CdTe–CdSe interface, particularly regarding interface roughness, are complicated issues. However, we suspect that the probability of the formation of the first monolayer led to the largest PL efficiency (QY  $\sim 38\%$ ), based on the fact that the PL efficiency of the resulting nanocrystals increased for  $\approx 3.5$  h (with an associated red shift of 53 nm), and the CdSe shell thickness of the core–shell nanocrystals grown for 3.5 h is 0.4–0.5 nm (as indicated by TEM). With an assumption of epitaxial growth, further growth of the CdSe shell caused a decrease of the PL efficiency; such a decrease can be overcome by growing another higher-bandgap material, such as ZnTe.<sup>[6]</sup> The growth of CdSe onto the CdTe core is always accompanied by significant red shifts in the PL peak position of the resulting nanocrystals; a further increase in the thickness of the CdSe allows the capability of tuning the heterostructured nanocrystal bandgap into the near-IR and IR spectral ranges. It should be pointed out that for type I CdSe/ZnS core–shell nanocrystals, the highest QYs were achieved with a ZnS coating of  $\approx 1.3$  monolayers on CdSe nanocrystals.<sup>[2b, 3, 18]</sup>

## 4. Conclusions

In conclusion, our synthetic approach, which starts with good quality CdTe nanocrystals and involves the sequential addition of shell-precursor solutions, is well suited to the fabrication of type II CdTe/CdSe nanocrystals with high PL efficiency. The approach precludes the formation of CdSe nanocrystals through careful selection of the shell-precursor quantity, injection temperature, and shell-growth temperature.

## Experimental Section

For the reaction results shown in Figure 2, 25.68 mg CdO (0.2 mmol) and 1.109 g TOP were loaded into a 25 mL three-necked flask and heated to 320 °C in air for about 2 h; usually, the CdO was completely dissolved at  $\approx 280$  °C. Afterwards, the

colorless solution was cooled to 300 °C under N<sub>2</sub> flow. Two stock solutions were prepared: stock solution 1 consisted of 12.76 mg Te (0.1 mmol) and 798.1 mg TOP. Stock solution 2 (1.67 g) had a Se concentration of  $\approx 59$  mmol kg<sup>-1</sup>. This solution was prepared by the addition of a TOPSe/TOP solution, consisting of 7.88 mg Se (0.1 mmol) and 169.87 mg TOP, into a Cd precursor solution in TOP, comprising 12.86 mg CdO (0.1 mmol) and 1.496 g TOP; the Cd precursor/TOP solution was prepared as described above, but the solution was cooled to 50 °C instead of 300 °C. Stock solution 2 was maintained at  $\approx 50$  °C. Table 1 summarizes the stock solutions that were prepared in this study (stock solutions 2–4 were prepared in a similar way).

Stock solution 1 was swiftly injected into the reaction flask containing the CdO/TOP solution at 300 °C under N<sub>2</sub> flow; the total mass was thus  $\approx 1.91$  g, with a Te concentration of  $\approx 52$  mmol kg<sup>-1</sup>. Afterwards, the reaction temperature was set at  $\approx 250$  °C for about 15 min for the growth of CdTe nanocrystals. Afterwards, the CdTe solution was cooled to 150 °C (over 14 min). After stock solution 2 was added dropwise, the reaction solution was heated up from 140 to 200 °C over a period of about 1 h.

To monitor the temporal evolution of the optical properties of the growing nanocrystals, aliquots of the reaction solution were removed at different intervals and kept in vials; afterwards a volume (10  $\mu$ L) of each sample was dispersed into 2 mL of hexanes, and the UV and PL properties of the dispersions were studied at room temperature. UV spectra were acquired on a Perkin Elmer Lambda 45 UV/vis spectrometer, and the PL spectra were acquired on a Fluoromax-3 spectrometer (Jobin Yvon Horiba, Instruments SA) with a 450 W Xe lamp as the excitation source and an excitation wavelength of 500 nm if not specified. Under our experimental approach, CdSe nanocrystals usually exhibit photoluminescence at wavelengths longer than 530 nm;<sup>[7]</sup> thus, the 500 nm excitation wavelength with PL spectra acquired between 510–900 nm is powerful enough to detect the possible formation of the CdSe nanocrystals. The recorded emission spectra of our nanocrystals were m-corrected, regarding the sensitivity of the detector response to emission wavelength, by using the manufacturer's procedure.

It is interesting to point out the detailed synthetic conditions for the core–shell nanocrystals shown in Figure 4: after obtaining curve 2, the reaction flask was cooled down to room temperature and protected under N<sub>2</sub>; after two days, the CdTe/CdSe nanocrystals exhibited similar PL properties, particularly with regard to the PL efficiency and peak position. Thus, we prepared stock solution 4, which was the same as stock solution 3. This solution was injected dropwise into the reaction flask at  $\approx 130$  °C; afterwards, the reaction flask was heated to 200 °C over 1.3 h. Between the 2 h to 3.5 h growth period, a red shift of only 3 nm was detected (the 3.5 h sample is shown as curve 3). Consequently, the flask was heated, and the 7 h (225 °C) and 13 h (238 °C) samples are shown as curves 4 and 5.

The TEM samples were prepared by several rounds of precipitation of the nanocrystals from THF/MeOH solutions followed by dispersing the nanoparticle precipitate in acetone and sonicating the resulting suspension for a few minutes; one drop of the sonicated suspension with finely separated nanocrystals was deposited onto a carbon-coated 300-mesh TEM copper grid and the dried grid was loaded into a double-tilt sample holder. The

TEM samples were examined on a Philips CM20 STEM equipped with a Gatan UltraScan 1000 CCD camera; the TEM was operated at 200 kV.

Powder X-ray diffraction (XRD) patterns were obtained from the nanoparticle precipitate (after repeated solvent/nonsolvent (THF/MeOH) precipitations). The XRD samples were prepared by the evaporation of THF and MeOH from the nanocrystals/THF/MeOH suspensions loaded on low-background glass plates. Diffraction patterns were recorded at room temperature on a Scintag XDS2000 diffractometer, using graphite-monochromatized  $\text{Cu}_{\text{K}\alpha}$  radiation ( $\lambda = 1.79 \text{ \AA}$ ) in the  $\theta$ - $\theta$  mode. Samples were usually scanned over a range of  $2^\circ < 2\theta < 60^\circ$  at an increment of  $0.5^\circ \text{ min}^{-1}$ , giving a total acquisition time of  $\approx 2 \text{ h}$ .

- 
- [1] a) H. Weller, *Adv. Mater.* **1993**, *5*, 88; b) V. L. Colvin, M. C. Schlamp, A. P. Alivisatos, *Nature* **1994**, *370*, 354; c) W. C. W. Chan, S. Nie, *Science* **1998**, *281*, 2016; d) A. J. Nozik, *Phys. E* **2002**, *14*, 115.
- [2] a) M. A. Hines, P. Guyot-Sionnest, *J. Phys. Chem.* **1996**, *100*, 468; b) X. Peng, M. C. Schlamp, A. V. Kadavanich, A. P. Alivisatos, *J. Am. Chem. Soc.* **1997**, *119*, 7019; c) B. O. Dabbousi, J. Rodriguez-Viego, F. V. Mikulec, J. R. Heine, H. Mattoussi, R. Ober, K. F. Jensen, M. G. Bawendi, *J. Phys. Chem. B* **1997**, *101*, 9436; d) Y. W. Cao, U. Banin, *Angew. Chem.* **1999**, *111*, 3913–3916; *Angew. Chem. Int. Ed.* **1999**, *38*, 3692.
- [3] A. Eychmüller, *J. Phys. Chem. B* **2000**, *104*, 6514.
- [4] J. Haetty, E. H. Lee, H. Luo, A. Petrou, J. Warnock, *Solid State Commun.* **1998**, *108*, 205.
- [5] S. H. Wei, A. Zunger, *Appl. Phys. Lett.* **1998**, *72*, 2011.
- [6] S. Kim, B. Fisher, H. J. Eisler, M. G. Bawendi, *J. Am. Chem. Soc.* **2003**, *125*, 11466.
- [7] K. Yu, S. Singh, N. Patrito, V. Chu, *Langmuir* **2004**, *20*, 11161.
- [8] Z. Zhu, H. Yoshihara, K. Takebayashi, T. Yao, *J. Cryst. Growth* **1994**, *138*, 619.
- [9] a) H. L. Hsieh, R. P. Quirk, *Anionic Polymerization*, Marcel Dekker, New York, **1996**; b) G. Liu, *Curr. Opin. Colloid Interface Sci.* **1998**, *3*, 200–208.
- [10] a) K. S. Kazanskii, A. A. Solovyanov, S. G. Eutelis, *Eur. Polym. J.* **1971**, *7*, 142; b) J. J. O'Malley, R. H. Marchessault, *Macromol. Synth.* **1972**, *4*, 35.
- [11] a) L. Zhang, K. Yu, A. Eisenberg, *Science* **1996**, *272*, 1777; b) K. Yu, C. Bartels, A. Eisenberg, *Langmuir* **1999**, *15*, 7157–7167.
- [12] a) D. V. Talapin, A. L. Rogach, E. V. Shevchenko, A. Kornowski, M. Haase, H. Weller, *J. Am. Chem. Soc.* **2002**, *124*, 5782; b) M. L. Steigerwald, L. E. Brus, *Annu. Rev. Mater. Sci.* **1989**, *19*, 471; c) W. W. Yu, A. Wang, X. Peng, *Chem. Mater.* **2003**, *15*, 4300.
- [13] J. Singh, K. K. Bajaj, S. Chaudhuri, *Appl. Phys. Lett.* **1984**, *44*, 805.
- [14] a) M. Nirmal, C. B. Murray, M. G. Bawendi, *Phys. Rev. B* **1994**, *50*, 2293; b) M. Kuno, J. K. Lee, B. O. Dabbousi, F. V. Mikulec, M. G. Bawendi, *J. Chem. Phys.* **1997**, *106*, 9869.
- [15] We tested the stability of the CdTe/CdSe nanocrystals (Figure 4; curve 2) solution in TOP: the reaction flask was cooled down to room temperature and protected under  $\text{N}_2$ ; after two days, the CdTe/CdSe nanocrystals exhibited similar PL properties, especially regarding the PL intensity and peak position.
- [16] "Optoelectronic Properties of Semiconductors and Superlattices": M. C. Tamargo in *II-VI Semiconductor Materials and Their Applications*, Sheridan, Ann Arbor, **2002**. p. 118. This reports wurtzite CdSe:  $a = 0.430 \text{ nm}$  and  $c = 0.7013 \text{ nm}$ ; wurtzite CdTe:  $a = 0.4572 \text{ nm}$  and  $c = 0.7484 \text{ nm}$ .
- [17] D. Battaglia, J. J. Li, Y. Wang, X. Peng, *Angew. Chem.* **2003**, *115*, 5189–5193; *Angew. Chem. Int. Ed.* **2003**, *42*, 5035.
- [18] With a 1.3 monolayer coating, surface Se valences of the initial CdSe core were saturated completely; further coating led to a decrease of PL efficiency due to stacking faults.<sup>[2b,3]</sup> Moreover, increases in both size distribution and aspect ratio (length/width) were also observed along with increased coating.<sup>[2b,3]</sup> It is a challenge to engineer rational experimental conditions, such as shell-growth temperature and concentration, to minimize such increases in size distribution and aspect ratio.

Received: September 7, 2004

Published online on December 21, 2004